Full dimensional Franck-Condon factors for the acetylene [~ over A] [superscript 1]A[subscript u] — [~ over X] [superscript 1#[+ over g] transition. II. Vibrational overlap factors for levels involving excitation in ungerade modes

Citation: Park, G. Barratt, Joshua H. Baraban, and Robert W. Field. "Full Dimensional Franck-Condon Factors for the Acetylene [~ over A] [superscript 1]A[subscript u] — [~ over X] [superscript 1]Σ[+ over g] Transition. II. Vibrational Overlap Factors for Levels Involving Excitation in Ungerade Modes." The Journal of Chemical Physics 141, no. 13 (October 7, 2014): 134305. © 2014 AIP Publishing LLC

As Published: http://dx.doi.org/10.1063/1.4896533

Publisher: American Institute of Physics (AIP)

Persistent URL: http://hdl.handle.net/1721.1/96883

Version: Final published version: final published article, as it appeared in a journal, conference proceedings, or other formally published context

Full dimensional Franck-Condon factors for the acetylene $\tilde{A}\ ^1A_u$—$\tilde{X}\ ^1\Sigma_g^+$ transition. II. Vibrational overlap factors for levels involving excitation in *ungerade* modes

G. Barratt Park,[a] Joshua H. Baraban,[b] and Robert W. Field
Department of Chemistry, Massachusetts Institute of Technology, Cambridge, Massachusetts 02139, USA

(Received 12 May 2014; accepted 15 September 2014; published online 3 October 2014)

A full-dimensional Franck-Condon calculation has been applied to the $\tilde{A}\ ^1A_u$—$\tilde{X}\ ^1\Sigma_g^+$ transition in acetylene in the harmonic normal mode basis. Details of the calculation are discussed in Part I of this series. To our knowledge, this is the first full-dimensional Franck-Condon calculation on a tetra-atomic molecule undergoing a linear-to-bent geometry change. In the current work, the vibrational intensity factors for levels involving excitation in *ungerade* vibrational modes are evaluated. Because the Franck-Condon integral accumulates away from the linear geometry, we have been able to treat the out-of-plane component of trans bend (ν_4'') in the linear $\tilde{X}$ state in the rotational part of the problem, restoring the χ Euler angle and the *a*-axis Eckart conditions. A consequence of the Eckart conditions is that the out-of-plane component of ν_4'' *does not participate* in the vibrational overlap integral. This affects the structure of the coordinate transformation and the symmetry of the vibrational wavefunctions used in the overlap integral, and results in propensity rules involving the bending modes of the $\tilde{X}$ state that were not previously understood. We explain the origin of some of the unexpected propensities observed in IR-UV laser-induced fluorescence spectra, and we calculate emission intensities from bending levels of the $\tilde{A}$ state into bending levels of the $\tilde{X}$ state, using normal bending mode and local bending mode basis sets. Our calculations also reveal Franck-Condon propensities for the Cartesian components of the cis bend (ν_5''), and we predict that the best $\tilde{A}$-state vibrational levels for populating $\tilde{X}$-state levels with large amplitude bending motion localized in a single C–H bond (the acetylene↔vinylidene isomerization coordinate) involve a high degree of excitation in ν_6' (cis-bend). Mode ν_4' (torsion) populates levels with large amplitude counter-rotational motion of the two hydrogen atoms. © *2014 AIP Publishing LLC*. [http://dx.doi.org/10.1063/1.4896533]

I. INTRODUCTION

The $\tilde{A}\ ^1A_u(C_{2h})$—$\tilde{X}\ ^1\Sigma_g^+(D_{\infty h})$ transition in acetylene has received extensive attention[1–37] because it was the first molecular system in which a qualitative change in geometry and symmetry accompanying an electronic excitation was proven by spectroscopic methods.[1–3] Of particular interest to the chemical community are the acetylene↔vinylidene[27,38–41] and cis↔trans[37,42–45] isomerizations that take place on the $\tilde{X}$-state and $\tilde{A}$-state surfaces, respectively. Because so much detailed work has been done on these electronic states, acetylene is a prototype for studying the spectroscopic signatures of isomerizing systems and the vibrational dynamics that occur at chemically interesting regions of the potential surface. Considerable work has been done by the Field group and collaborators to find Stimulated Emission Pumping (SEP) and Dispersed Fluorescence (DF) schemes for populating levels of the $\tilde{X}$ state relevant to the acetylene↔vinylidene isomerization. However, highly excited vibrational levels in the vicinity of reaction barriers are difficult to access because most of the amplitude of the vibrational wavefunction is at geometries far from equilibrium. This has motivated our calculation of full-dimensional Franck-Condon factors for the $\tilde{A}$—$\tilde{X}$ system.

The method used to calculate full-dimensional Franck-Condon factors is detailed in Part I of this series. This paper is intended to be accessible to those who have not read Part I, but readers should be aware of the following details of the calculation.

1. The vibrational overlap integrals are performed in the harmonic normal mode basis, using a curvilinear coordinate transformation. There are quantitative discrepancies between the calculated and observed intensities. Most notably, the calculation underestimates the overall oscillator strength for the vibrationless 0–0 intensity by ∼3 orders of magnitude. The most likely explanation is that the large amplitude displacement along the trans-bend coordinate between the equilibrium geometries of the $\tilde{A}$ and $\tilde{X}$ states is not well described by the harmonic treatment, which is expected to give quantitative results only at small amplitudes. As shown in Part I, the 0–0 vibrational overlap depends sensitively on the displacement between the equilibrium geometries. In spite of this discrepancy, the qualitative trends in calculated FC factors are in agreement with the experimental observations, especially for progressions involving the trans-bending mode, and we believe that the calculations yield

[a]Electronic mail: barratt@mit.edu
[b]Present address: Department of Chemistry and Biochemistry, University of Colorado Boulder, Boulder, Colorado 80309-0215, USA.

qualitatively accurate and meaningful trends, when normalized to the 0–0 intensity. It is likely that higher-order calculations that take into account vibrational anharmonicity will succeed at achieving better quantitative results, but these are beyond the scope of the current work.

2. The angular component of the doubly-degenerate trans bend (ν_4'') in the linear $\tilde{X}$ state has been treated as a rotation. The wavefunction used for this doubly degenerate mode has the form shown in Eq. (68) of Part I of this series. The angular factor $\exp(il_4\phi_4)$ is excluded from the vibrational integral and is treated instead in the rotational integral. This treatment is valid because most of the FC integral accumulates away from the linear geometry. As shown in Sec. II C of Part I, the vibrational coordinates of the $\tilde{X}$ state satisfy rotational Eckart conditions for the *a*-axis, and the treatment is equivalent to constraining the vibrational coordinate q_4'' to lie in the plane of the equilibrium geometry of the trans-bent $\tilde{A}$ state. An important consequence is that the out-of-plane component of ν_4'' *does not contribute* to vibrational overlap with the $\tilde{A}$ state. This fact plays a major role in the vibrational propensities, discussed in Secs. IV and V of this paper.
3. In Part I, we found that a curvilinear formulation of the normal mode coordinate transformation provides better agreement with experiment than the coordinate transformation used by Watson,[46] which involves rectilinear normal mode coordinates with a first-order correction for axis-switching effects. The improvement is most profound for the bending progressions in ν_4''. We also found that the newer $\tilde{A}$-state force field parameters of Ref. 47 provide better agreement with experimental intensities than the parameters of Ref. 48. In the present paper, we provide a brief comparison in Sec. III A between the performance of the curvilinear coordinate transformation (Table VIII of Part I) and the rectilinear transformation with corrections for axis-switching (Table VI of Part I). The subsequent calculations in Secs. III B–V use the curvilinear transformation exclusively.

In this work, we apply the methods described in Part I to calculate vibrational intensity factors for levels of the acetylene $\tilde{A}$–$\tilde{X}$ system that involve excitation in *ungerade* modes. In Sec. III, we compare our results to experimentally-determined intensities from IR-UV double resonance pumped DF measurements.[28] In Sec. IV, we use our calculation to explain experimentally observed propensities in IR-UV pumped laser induced fluorescence experiments. Finally, in Sec. V, we perform a normal to local mode basis transformation and apply our results to the problem of accessing large amplitude local-bending bright states relevant to the acetylene↔vinylidene isomerization.

II. POLYAD STRUCTURE AND BENDING DYNAMICS IN THE $\tilde{A}$—$\tilde{X}$ SYSTEM

The acetylene↔vinylidene isomerization that occurs on the $\tilde{X}$-state surface and the cis↔trans isomerization that occurs on the $\tilde{A}$-state surface both involve primarily bending degrees of freedom. We will therefore provide some background on the properties of bending vibrations in acetylene, and how the bending modes relate to overall vibrational polyad structures. The frequencies, symmetries, and descriptions of the normal modes of the $\tilde{X}$ and $\tilde{A}$ states are summarized in Tables II and III, respectively, of Part I of this series.

A. $\tilde{X}$-state polyad structure

The vibrational Hamiltonian of the $\tilde{X}$ state of acetylene is known to be approximately block diagonal in the polyad-forming quantum numbers

$$N_s = v_1'' + v_2'' + v_3'', \tag{1}$$

$$N_{\text{res}} = 5v_1'' + 3v_2'' + 5v_3'' + v_4'' + v_5'', \tag{2}$$

$$l = l_4 + l_5, \tag{3}$$

up to energies of at least 15 000 cm^{-1}.[27] In this paper, polyads of the $\tilde{X}$ state will be identified by the shorthand notation $\{N_s, N_{\text{res}}, l\}$, followed by a $D_{\infty h}$ vibrational symmetry label. The zero-order states that comprise each polyad are notated $(v_1, v_2, v_3, v_4^{l_4}, v_5^{l_5})$. These basis states have well-defined *g*/*u* symmetry and may be symmetrized to have well-defined +/− total parity. The parity and *g*/*u* symmetry are conserved by the vibrational Hamiltonian, and are therefore also conserved within each polyad.

In the absence of excitation in the stretching modes, $N_s = 0$ and the bending modes $\nu_4''(\pi_g)$ and $\nu_5''(\pi_u)$ form pure bending polyads with conserved polyad numbers

$$N_B = N_{\text{res}} = v_4'' + v_5'', \tag{4}$$

$$l = l_4 + l_5. \tag{5}$$

As we shall see in Sec. V, the pure bending polyads may be described in the basis of normal modes, as above, or in the basis of local bending modes. At high quanta of bending excitation, the local modes become a better zero-order description of the vibrational eigenstates.[49] In the absence of axis-switching, the selection rule for *l* arises from the *c*-axis electronic transition moment for the $\tilde{A}$—$\tilde{X}$ system, which leads to $K' - l'' = \pm 1$ for the projection of angular momentum on the *a*-axis.

B. Bending modes of the $\tilde{A}$ state

The torsion $\nu_4'(a_u)$ and cis-bending $\nu_6'(b_u)$ modes of the $\tilde{A}$ state are near-degenerate and interact through strong Darling-Dennison[35,36] and Coriolis resonances.[31] In this paper, we refer to polyads with $v_4' + v_6' = n$ as B^n. Modes ν_4' and ν_6' correlate with the out-of-plane and in-plane components, respectively, of the $\tilde{X}$-state cis-bend, ν_5''. This gives rise to a Franck-Condon propensity $v_5'' = v_4' + v_6'$ in the $\tilde{A}$—$\tilde{X}$ spectrum.

Because of the large displacement in the trans-bend coordinate between the $\tilde{A}$- and $\tilde{X}$-state equilibrium geometries, there is a strong Franck-Condon intensity progression in the trans-bending mode, $\nu_3'(a_g)$. The trans-bend is higher

in frequency than ν_4' and ν_6' and does not interact strongly with the B^n polyads at low vibrational quanta. However, the cis-trans isomerization gives rise to very strong negative anharmonicity between modes ν_3' and ν_6' because the in-plane isomerization coordinate is a combination of q_3' and q_6'. Therefore, in combination levels $3^m B^n$, mode ν_3' effectively tunes ν_6' out of resonance with ν_4' and weakens the intrapolyad interactions.[36,42–44,50]

III. DISPERSED FLUORESCENCE FROM $\tilde{A}(3^m6^1)$

A. The $\tilde{A}(3^m6^1) \rightarrow \tilde{X}(0, v_2, 0, v_4^{+1}, 1^{-1})\Sigma_u^+$ progressions

In Figure 1, calculated emission intensities to the dominant progressions observed from $2\nu_3' + \nu_6'$ and $3\nu_3' + \nu_6'$ to $\tilde{X}(0, v_2, 0, v_4^{+1}, 1^{-1})\Sigma_u^+$ are compared with experimental observations obtained from DF measurements by Hoshina *et al.*[28] In the experiment, *ungerade* ($K'_{K'_a,K'_c} = 1_{1,0}, e$) levels of the $\tilde{A}$ state were excited by a two-photon scheme, via the $\nu_3''(\sigma_u^+)$ intermediate state. The fluorescence was dispersed onto a CCD detector attached to a monochromator, and the relative intensities in each emission spectrum were calibrated by dispersing a halogen lamp onto the same detector. Only the relative FC intensities within each emission spectrum are reported—the relative intensities between different emission spectra are uncertain due to power variation and fluctuation in the lasers used to pump the excited state. Therefore, the experimental data and calculated intensities shown in Figure 1 are all consistently normalized to the strongest transition in the first lobe of the v_4'' progression.

The calculation places the maximum in the v_2'' progression at 0–1 quanta, whereas the observed maximum is at 2 quanta. In the v_4'' progressions, the calculated location of the first node is in good qualitative agreement with experiment. The calculation places the first node in fluorescence from $2\nu_3' + \nu_6'$ at $v_4'' = 13$ and the first node in fluorescence from $3\nu_3' + \nu_6'$ at $v_4'' = 11$, whereas in the experiment the nodes are observed at $v_4'' = 11$ and $v_4'' = 9$, respectively. This shift that occurs in the node position when the upper level is changed from $2\nu_3' + \nu_6'$ to $3\nu_3' + \nu_6'$ reflects a shift in the first node position along the trans-bend coordinate of the upper state wavefunction. The experimental DF spectra did not extend sufficiently high in energy to determine the locations of higher-lying nodes. As with dispersed fluorescence data from *gerade* levels of the $\tilde{A}$ state (shown in Part I of this series), the curvilinear coordinate transformation does a better job at reproducing the observed intensity at high quanta in v_4''.

B. Multiple zero-order bright states in spectra from $\tilde{A}$-state 3^m6^1

Hoshina and co-workers[28] also report interference effects from multiple zero-order bright states in the DF spectra from the *ungerade* $\tilde{A}$-state levels 3^26^1 and 3^36^1. As mentioned in Sec. II A, the Franck-Condon propensity rule for the cis-bending mode v_5'' is that the nominal zero-order bright states

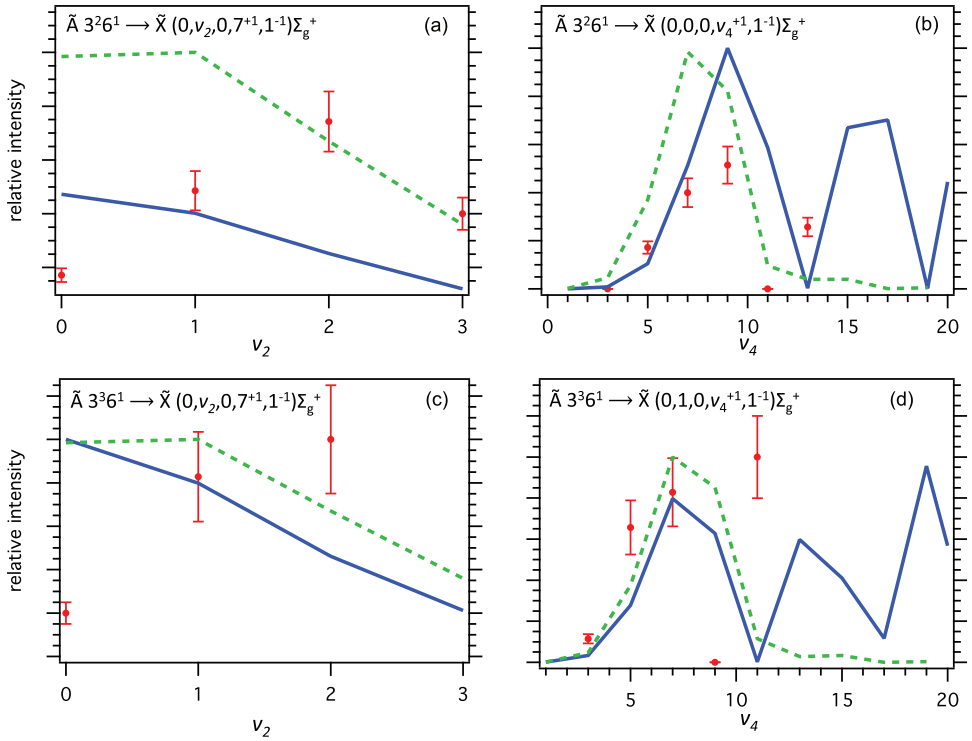

FIG. 1. Relative emission intensities for $\tilde{A}(3^m6^1)(b_u)$ to zero-order bright states $\tilde{X}(0, v_2, 0, v_4^{+1}, 1^{-1})\Sigma_u^+$ of acetylene. Emission is shown from $\tilde{A}(3^26^1)$ (panels (a) and (b)) and $\tilde{A}(3^36^1)$ (panels (c) and (d)). Panels (a) and (c) display progressions in v_2'' ($v_4'' = 7$ and $v_5'' = 1$), and panels (b) and (d) display progressions in v_4'' ($v_2'' = 0$ or 1, $v_5'' = 1$). Representative progressions were chosen based on the best availability of experimental data for comparison. Experimental intensities from IR-UV-DF measurements[28] are displayed as points with 15% uncertainty. The observed and calculated intensities from both emission spectra are normalized relative to the strongest transition in the first lobe of the v_4'' progression. The calculations were performed with a curvilinear coordinate transformation (solid blue curve) and a rectilinear coordinate transformation with first-order corrections for axis switching (dotted green curve).

(ZOBSs) should conserve the quanta of $v_5'' = v_4' + v_6'$. Furthermore, because the $\tilde{A} \leftarrow \tilde{X}$ transition involves little change in the symmetric CH stretch frequencies, v_1'' and v_1', the antisymmetric stretch frequencies, v_3'' and v_5', *or* the equilibrium C—H bond length, there are additional FC propensity rules for $v_1'' = v_1'$ and $v_3'' = v_5'$ to be conserved.

Within each polyad with given values of $N_s = v_2''$ and N_{res}, defined in Eqs. (1)–(3), there is only one nominal zero-order state that is bright in each Σ_u^+ polyad: $(0, v_2'', 0, v_4''^{+1}, 1^{-1})\Sigma_u^+$, and there are two nominal zero-order bright states in each Δ_u polyad: $(0, v_2'', 0, v_4''^{+1}, 1^{+1})\Delta_u$ and $(0, v_2'', 0, v_4''^{+3}, 1^{-1})\Delta_u$. (Throughout this section, the zero-order Σ states are assumed to be symmetrized so that the total parity is +, i.e., $(0, v_2'', 0, v_4''^{+1}, 1^{-1})\Sigma_u^+$ is shorthand for the symmetric linear combination $(1/\sqrt{2})[(0, v_2'', 0, v_4''^{+1}, 1^{-1}) + (0, v_2'', 0, v_4''^{-1}, 1^{+1})]$.) For this nominally bright class of states, the number of quanta in v_4'' is given by $v_4'' = N_{res} - 3N_s - 1$.

However, the observed interference effects suggest that there is an *additional* class of zero-order bright state contributing to the intensity in the emission spectra. The authors of Ref. 28 find strong evidence that the interfering class of zero-order states are of the type $(0, \{v_2'' - 1\}, 1, \{v_4'' - 1\}^0, 0^0)\Sigma_u^+$ or $(0, \{v_2'' - 1\}, 1, \{v_4'' - 1\}^{+2}, 0^0)\Delta_u$, which is bright due to Duschinsky rotation between the b_u vibrational modes. To obtain this new class of ZOBS, we have exchanged $v_2'' + v_4'' + v_5''$ for v_3''. Reference 28 reports the ratio of emission intensities obtained by fitting the observed interference patterns to an effective Hamiltonian polyad model for the $\tilde{X}$ state.

Table I lists the calculated and experimentally determined intensity ratios for emission from 3^m6^1 levels of the $\tilde{A}$ state into the nominally allowed zero-order Δ_u states with different combinations of $l_4 + l_5 = 2$: $(0, v_2'', 0, v_4''^{+1}, 1^{+1})\Delta_u$ and $(0, v_2'', 0, v_4''^{+3}, 1^{-1})\Delta_u$. The calculated and observed values are all on the same order of magnitude, ranging from ~0.05 to 0.5. The calculation places slightly higher relative intensity into the $(0, v_2'', 0, v_4''^{+3}, 1^{-1})\Delta_u$ states than is observed. However, both the calculation and the experimental observations find that the ratio increases with increasing quanta in v_4''.

Tables II and III list the calculated and experimentally determined intensity ratios for emission from 3^m6^1 levels of the $\tilde{A}$ state into the nominally bright zero-order *ungerade* states, $(0, v_2, 0, v_4, 1)$, and into the FC propensity forbidden zero-order states, $(0, \{v_2 - 1\}, 1, \{v_4 - 1\}, 0)$ with $l = 2$ or 0. The calculated and observed intensity ratios are all on an order of magnitude ranging from $\sim 10^{-3}$ to 10^{-2}, and exhibit an increasing trend with increasing N_{res}. The qualitative agreement between experiment and calculation provides strong evidence that our calculations do a good job of reproducing the magnitudes of Duschinsky rotation effects, and that the model used by Hoshina *et al.*,[28] correctly identified which class of zero-order states is responsible for the interference effect. The calculated ratios are, on average, slightly smaller than the experimental ratios, indicating that the calculation may underestimate the degree of Duschinsky rotation of the b_u modes.

The calculated intensity ratios reported in Tables II and III were obtained using the curvilinear coordinate transformation described in Part I of this series. (See Table VIII of Part I.) In this transformation, the Duschinsky rotation is described by the relationship $\bar{q}_6' = 1.03\bar{q}_{5b}'' + 0.0176\bar{q}_3''$, or a rotation of ~2% between the b_u vibrational modes. We note that the Duschinsky rotation matrix elements obtained from the rectilinear coordinate transformation (Tables VI and VII of Part I) are larger by an order of magnitude (~40% rotation). Intensity calculations based on the rectilinear coordinate transformations overestimate the observed intensity ratios in Tables II and III *by two orders of magnitude*. This

TABLE I. The FC intensity ratio for emission from $\tilde{A}$ 3^m6^1 into $(0, v_2, 0, v_4^{+3}, 1^{-1})\Delta_u$ and $(0, v_2, 0, v_4^{+1}, 1^{+1})\Delta_u$ levels of the $\tilde{X}$ state. The ratio is calculated from $|\langle 3^m6^1|q_{4b}''|(0, v_2, 0, v_4^{+3}, 1^{-1})\rangle : \langle 3^m6^1|q_{4b}''|(0, v_2, 0, v_4^{+1}, 1^{+1})\rangle|^2$. The uncertainty in the experimentally observed ratios is estimated to be ~20%.

$\tilde{X}$-state polyad			Upper level:	3^26^1		3^36^1	
$\{N_s, N_{res}, l\}$	v_2''	v_4''	Ratio:	Calc.	Expt.[a]	Calc.	Expt.[a]
$\{0, 4, 2\}\Delta_u$	0	3		0.16		0.17	
$\{0, 6, 2\}\Delta_u$	0	5		0.36	0.13	0.38	0.28
$\{0, 8, 2\}\Delta_u$	0	7		0.52	0.18	0.56	0.31
$\{1, 7, 2\}\Delta_u$	1	3		0.16	0.058	0.17	0.10
$\{1, 9, 2\}\Delta_u$	1	5		0.36	0.090	0.38	0.18
$\{1, 11, 2\}\Delta_u$	1	7		0.52	0.12	0.56	0.30

[a]Reference 28.

TABLE II. The FC intensity ratio for emission from $\tilde{A}$ 3^m6^1 into $(0, 1, 0, v_4^{+1}, 1^{+1})\Delta_u$ and $(0, 0, 1, \{v_4 - 1\}^{+2}, 0^0)\Delta_u$ levels of the $\tilde{X}$ state. Intensity into the latter class of zero-order state arises from Duschinsky rotation between the b_u vibrational modes. The ratio is calculated from $|\langle 3^m6^1|q_{4b}''|(0, 0, 1, \{v_4 - 1\}^{+2}, 0^0)\rangle : \langle 3^m6^1|q_{4b}''|(0, 1, 0, v_4^{+1}, 1^{+1})\rangle|^2$. The uncertainty in the experimentally observed ratios is estimated to be ~20%.

$\tilde{X}$-state polyad		Upper level:	3^26^1		3^36^1	
$\{N_s, N_{res}, l\}$	v_4''	Ratio ($\times 10^3$):	Calc.	Expt.[a]	Calc.	Expt.[a]
$\{1, 7, 2\}\Delta_u$	3		0.38	1.0	0.47	7.6
$\{1, 9, 2\}\Delta_u$	5		1.0	3.1	1.3	3.1
$\{1, 11, 2\}\Delta_u$	7		2.0	3.0	2.7	6.5
$\{1, 13, 2\}\Delta_u$	9		3.5		6.5	

[a]Reference 28.

TABLE III. The FC intensity ratio for emission from $\tilde{A}$ 3^m6^1 into $(0, 1, 0, v_4^{+1}, 1^{-1})\Sigma_u^+$ and $(0, 0, 1, \{v_4 - 1\}^0, 0^0)\Sigma_u^+$ levels of the $\tilde{X}$ state. Intensity into the latter class of zero-order state arises from Duschinsky rotation between the b_u vibrational modes. The ratio is calculated from $|\langle 3^m6^1|q_{4b}''|(0, 0, 1, \{v_4 - 1\}^0, 0^0)\rangle : \langle 3^m6^1|q_{4b}''|(0, 1, 0, v_4^{+1}, 1^{-1})\rangle|^2$. The uncertainty in the experimentally observed ratios is estimated to be ~20%.

$\tilde{X}$-state polyad		Upper level:	3^26^1		3^36^1	
$\{N_s, N_{res}, l\}$	v_4''	Ratio ($\times 10^3$):	Calc.	Expt.[a]	Calc.	Expt.[a]
$\{1, 5, 0\}\Sigma_u^+$	1		0.87		1.0	
$\{1, 7, 0\}\Sigma_u^+$	3		1.3	8.5	1.5	0.80
$\{1, 9, 0\}\Sigma_u^+$	5		1.9	2.0	2.4	2.3
$\{1, 11, 0\}\Sigma_u^+$	7		2.9	9.0	3.9	11.
$\{1, 13, 0\}\Sigma_u^+$	9		4.5	19.	8.1	

[a]Reference 28.

provides further evidence that the curvilinear formulation provides a more physically realistic description of the normal coordinate transformation for the $\tilde{A}$—$\tilde{X}$ transition in acetylene than the rectilinear formulation used by Watson.[46]

IV. PROPENSITIES IN IR-UV FLUORESCENCE

Merer and co-workers[35] note that the relative strengths of transitions to $\tilde{A}$-state $K' = 0$ levels with a_u and b_u vibrational symmetry depend on which $\tilde{X}$-state π_u intermediate level is used in the double resonance scheme. In their paper, they use the $\nu_3'' + \nu_4''$ intermediate and they note that transitions to b_u levels of the $\tilde{A}$-state are much more intense in the fluorescence spectrum than transitions to a_u levels. The authors mention that in experiments on other polyads via the $\nu_1'' + \nu_5''$ (π_u) intermediate, a_u levels are dominant in intensity. However, they remark that it was unclear to them why this dramatic difference in intensity patterns should occur.

Calculated Franck-Condon factors for transitions between each of these two π_u intermediate levels and members of the lowest-lying *ungerade* B^n polyads of the $\tilde{A}$ state are shown in Table IV. The intensities arising from each Cartesian component of ν_5'' (out-of-plane ν_{5x}'' versus in-plane ν_{5y}'') are shown separately. For transitions out of ν_4'', the Franck-Condon calculation only grants transition intensity from the in-plane component ν_{4y}'' because the *a*-axis Eckart constraint $\phi_4 = 0$ requires that the out-of-plane component ν_{4x}'' must transform like an *a*-axis rotation in C_{2h}. The ν_{4x}'' degree of freedom is included in the $\tilde{\mathbf{I}}_{\mathbf{R}}''$ matrix for rotations rather than the $\tilde{\mathbf{I}}''$ matrix for vibrations, and the Eckart conditions ensure that it does *not* contribute to vibrational overlap intensity.

This Eckart constraint explains the physical origin of the trend in intensities observed in Ref. 35 for double-resonance spectra obtained via the $\nu_3'' + \nu_4''$ (π_u) intermediate. When using the $\nu_3'' + \nu_4''$ intermediate level, all intensity must come from the in-plane component, ν_{4y}'', which has a_g symmetry in C_{2h}. Therefore, by symmetry, non-zero vibrational overlap may only occur between $\nu_3'' + \nu_4''$ and states of b_u vibrational symmetry. We should note that in the actual spectrum transition intensity from $\nu_3'' + \nu_4''$ into a_u levels will be non-zero due primarily to Coriolis interactions in the B^n polyads that are not treated here.

TABLE IV. Calculated Franck-Condon factors for transitions between zero-order members of the *ungerade* $\tilde{A}$-state B^n polyads and the π_u levels of the $\tilde{X}$-state used as pump states in IR-UV double resonance experiments. The values are given relative to the vibrationless 0–0 intensity.[35]

π_u Intermediate:		$\nu_1'' + \nu_{5x}''$	$\nu_1'' + \nu_{5y}''$	$\nu_3'' + \nu_{4y}''$
	$D_{\infty h}$:	$\sigma_g^+ \otimes \pi_u$	$\sigma_g^+ \otimes \pi_u$	$\sigma_u^+ \otimes \pi_g$
	C_{2h}:	$a_g \otimes a_u$	$a_g \otimes b_u$	$b_u \otimes a_g$
B^1	4^1 (a_u)	0.0683	0	0
	6^1 (b_u)	0	0.0680	0.0280
B^3	4^3 (a_u)	7.54×10^{-5}	0	0
	$4^2 6^1$ (b_u)	0	2.50×10^{-5}	1.03×10^{-5}
	$4^1 6^2$ (a_u)	3.85×10^{-5}	0	0
	6^3 (b_u)	0	1.15×10^{-4}	4.74×10^{-5}

On the other hand, $\nu_1'' + \nu_5''$ grants Franck-Condon access to both a_u and b_u vibrational levels. Access to a_u levels comes solely from the out-of-plane component, $\nu_1'' + \nu_{5x}''$, and access to b_u levels comes solely from the in-plane-component, $\nu_1'' + \nu_{5y}''$. In the B^1 polyad, the harmonic calculation predicts approximately equal intensity into the $\nu_4'(a_u)$ and $\nu_6'(b_u)$ levels. Because the harmonic frequencies of the zero-order members of the B^1 polyad are very nearly degenerate and the equilibrium displacement along *ungerade* normal mode coordinates is zero, we would not expect our harmonic intensity calculation to favor one plane of cis-bend motion over the other, so this result is not surprising. The very small intensity advantage of ν_4' over ν_6' comes from the isolation of the out-of-plane (a_u) block of the Duschinsky matrix. That is, ν_6' loses some of its intensity due to Duschinsky rotation in the b_u modes, whereas ν_4' is the only mode with a_u symmetry, so it does not experience any Duschinsky rotation. As mentioned in Sec. III B, the fact that the calculation underestimates the ratios reported in Tables II and III indicates that the calculation may underestimate the degree of b_u Duschinsky rotation, so that it overestimates the intensity from $\nu_1'' + \nu_5''$ into ν_6'. However, this effect is probably not large enough to explain the strongly observed propensities, and other anharmonic factors are probably at play.

There are two reasons why the $\nu_6'(b_u)$ level within each B^1 polyad is likely to undergo more severe anharmonic interactions with other levels than the $\nu_4'(a_u)$ level. First, the total density of b_u levels is higher than the density of a_u levels (because ν_5' also has b_u character). Second, anharmonic overlap is more likely between zero-order basis states that encode motion in the same plane. Other than $\nu_6'(b_u)$, there are four other in-plane vibrational modes, but there are no out-of-plane vibrational modes other than ν_4'. These anharmonic interactions will weaken the propensity for $\nu_{5y}'' = \nu_6'$, and might cause a_u levels to dominate in transitions from $\nu_1'' + \nu_5''$. Propensities for transitions from the $\nu_3'' + \nu_4''$ intermediate will not be affected by such anharmonic considerations, because the transition from $\nu_3'' + \nu_4''$ to all a_u levels are equally forbidden by the Eckart conditions.

The calculation does not in general find a strong preference for a_u levels over b_u levels in transitions to higher-lying B^n polyads. However, transitions from $\nu_1'' + \nu_5''$ to higher *ungerade* B^n polyads with $n \geq 3$ are very weak because they are forbidden by the Franck-Condon propensity $v_5'' = v_4' + v_6'$. The calculations in Table IV indicate that Franck-Condon access to B^3 is weaker than the FC access to B^1 by three orders of magnitude. Therefore, as mentioned in Ref. 35, the higher-lying *ungerade* B^n polyads observed in the spectra from the $\nu_1'' + \nu_5''$ intermediate probably borrow much of their intensity from anharmonic interactions with nearby $2^m 3^n B^1$ levels that are strongly allowed by the Franck-Condon propensities. Because anharmonic interactions preserve vibrational symmetry, a_u levels of higher-lying B^n polyads will borrow intensity from the $2^m 3^n 4^1$ (a_u) member of the nearby B^1 polyad and b_u levels will borrow intensity from the $2^m 3^n 6^1$ (b_u) member. If we assume that our calculation has overestimated the intensity from $\nu_1'' + \nu_5''$ to ν_6', then that will be sufficient to explain the general observation that a_u levels dominate in transitions from $\nu_1'' + \nu_5''$. For higher-lying *ungerade*

B^n polyads, the effect is largely via intensity borrowing from $2^m3^n4^1$ levels.

V. EMISSION FROM LEVELS OF *GERADE* B^n POLYADS TO BENDING LEVELS OF THE $\tilde{X}$ STATE

Extensive work by the Field lab and collaborators has focussed on the approach to the acetylene ⇌ vinylidene isomerization on the S_0 surface.[27] This has attracted interest to local bending modes of S_0, because the local bending motion lies along the reaction coordinate for the isomerization. Local bending in S_0 acetylene—where the bending motion is localized to a single CCH bond angle—is achieved through a one-to-one linear combination of modes ν_4'' and ν_5''. As discussed in Sec. II A, these modes form pure bending polyads with conserved polyad numbers $N_B = v_4'' + v_5''$ and $l = l_4 + l_5$. At low bending energies, the pure-bending polyad eigenstates are best described in the basis of trans-bend and cis-bend normal modes. The trans-bend is lower in frequency than the cis-bend, so levels with the most trans-bend character lie at the low energy extreme of the polyad and levels with the most cis-bend character lie at the high energy extreme of the polyad. Because the anharmonicities x_{44} and x_{55} have opposite signs, the trans and cis basis states converge as N_B increases. This causes strong Darling-Dennison interactions to turn on at $N_B \geq 12$, and new classes of motion emerge as a result. The pure-bending polyad structure rearranges itself so that the eigenstates are better described in the local mode basis. Jacobson *et al.*[49] have shown that for $l = 0$, large amplitude local bend levels fall to the low energy extreme of the polyad, and counter-rotating levels rise to the high energy extreme of the polyad. Tyng and Kellman have analyzed this normal mode bifurcation by semi-classical methods,[51] and they have released an excellent collection of animations that illustrate the classical motions that result.[52]

One of the most challenging experimental obstacles in observing zero-order large amplitude local bending states—which are a 1:1 admixture of cis- and trans-bending modes—is that FC propensities make it difficult to achieve bending excitation with a high degree of cis-bending character. One of the driving goals of the extensive characterization of the acetylene $\tilde{A}$ state has been to determine which "perfect pluck" vibrational levels will fluoresce to vinylidene-like local bending levels of the $\tilde{X}$ state. This problem has generated interest in members of the $\tilde{A}$-state B^n polyads because the ν_4' and ν_6' modes from which the polyads are composed correlate to the out-of-plane and in-plane components, respectively, of the $\tilde{X}$-state cis bend, ν_5''. The Franck-Condon propensity $v_5'' = v_4' + v_6'$ make the B^n polyads promising as candidates for intermediates in SEP or DF schemes for accessing ν_5'' character and reaching highly-excited local bending states of S_0.

However, the "perfect pluck" problem is not so simple as merely populating a zero-order bright state of S_0 with equal ν_4'' and ν_5'' character. In the high-lying pure bend polyads, there are many states that comprise the zero-order local mode product basis. Only a few of these states will contain the correctly-phased linear combination of zero-order *normal mode* product basis states to give rise to large-amplitude bending motion along the isomerization coordinate. The goal of this section is to understand the best strategy for reaching these zero-order levels.

A. Fluorescence intensities and phases for transitions into $\tilde{X}$-state pure bending polyads in the normal mode basis

A full table of calculated vibrational overlap integrals that connect zero-order members of the $\tilde{A}$-state *gerade* B^n polyads ($n = 0, 2, 4$) with members of $\tilde{X}$-state *gerade* pure-bending polyads ($N_B \leq 10$) in the harmonic normal mode basis may be found in the supplementary material.[53] There are a few important trends. First, overall brightness increases dramatically as N_B increases, primarily due to the strong FC progression in v_4''. At low N_B, as the number of quanta in B^n of the upper level increases, the overall fluorescence intensity into a given pure bending polyad of the $\tilde{X}$ state decreases. However, this trend begins to reverse at high quanta of excitation in the $\tilde{X}$-state pure-bending polyads. The propensity rule $v_5'' = v_4' + v_6'$ is fairly well obeyed within each ground state pure-bending polyad. From each B^n polyad, the vibrational overlap magnitude is strongly peaked at $\tilde{X}$-state levels $v_5'' = n$. The propensity rule is slightly relaxed for ν_6' relative to ν_4' as a result of the fact that ν_4' is the only out-of-plane mode, and overlaps very efficiently with ν_{5c}''. (The out-of-plane component of ν_4'' does not participate in the Franck-Condon intensities due to the Eckart constraint, so overlap between totally symmetric overtones of ν_4' and ν_{4c}'' do not contribute to vibrational intensities.) On the other hand, ν_6' may mix into ν_3'' in the coordinate transformation via Duschinsky rotation, and even quanta of ν_6' will have a small amount of overlap with totally symmetric combinations of in-plane modes of the $\tilde{X}$ state (such as even quanta of ν_{4b}''). As a result, the distribution of overlap from 6^n levels within each pure bending polyad of the $\tilde{X}$ state is less sharply peaked at $v_5'' = n$ than is the case for 4^n levels.

Table V lists a small subset of the vibrational overlap integrals printed in the supplementary material,[53] relevant to the emission from zero-order members of the $\tilde{A}$-state B^4 polyad to zero-order members of the $\tilde{X}$-state $N_B = 8$ pure bending polyad. Despite the fact that overlap from 6^n levels is less sharply peaked, the intensity distribution from 6^n closely resembles the distribution from 4^n. However, within pure bending polyads of the $\tilde{X}$ state, the *phases* of the overlap integrals with the various members of each B^n polyad *do not* resemble one another. The physical origin of this phenomenon comes from the fact that 4^n and 6^n place intensity into different Cartesian components of the ν_5'' two-dimensional harmonic oscillator. In the following discussion, we use y to label the in-plane components and x to label the out-of-plane components. The 6^n level will overlap predominantly with $|v_{5x}'', v_{5y}''\rangle = |0, n\rangle$, whereas 4^n will overlap predominantly with $|n, 0\rangle$. As a result of the Eckart constraint, all intensity from $\tilde{A} \rightarrow \tilde{X}$ emission goes into the in-plane component of ν_4''. Therefore, in the product basis of Cartesian two-dimensional harmonic oscillators, emission from 4^m6^n will fluoresce predominantly to

$$4^m6^n \rightarrow |v_{4x}'', v_{4y}''\rangle|v_{5x}'', v_{5y}''\rangle = |0, v_{4y}''\rangle|m, n\rangle \qquad v_{4y}'' = N_B - (n + m). \tag{6}$$

TABLE V. Calculated vibrational overlap integrals connecting zero-order members of the Ã-state *gerade* B^4 polyad with members of $\tilde{X}$-state $N_B = 8$ *gerade* pure-bending polyad in the harmonic normal mode basis.

$\tilde{X}$-state zero-order level			Ã-state B^4 polyad member				
N_B	l	$[v_4^{l_4}, v_5^{l_5}]$	6^4	$4^1 6^3$	$4^2 6^2$	$4^3 6^1$	4^4
8	0	$[8^0, 0^0]$	3.04×10^{-1}		2.01×10^{-1}		1.99×10^{-1}
		$[6^{+2}, 2^{-2}]$	3.98×10^{0}	$3.99i \times 10^{0}$	-3.18×10^{-1}	$3.22i \times 10^{0}$	-3.23×10^{0}
		$[6^0, 2^0]$	7.00×10^{0}		5.18×10^{0}		5.67×10^{0}
		$[4^{+4}, 4^{-4}]$	2.67×10^{0}	$5.35i \times 10^{0}$	-6.56×10^{0}	$-5.37i \times 10^{0}$	2.69×10^{0}
		$[4^{+2}, 4^{-2}]$	1.71×10^{1}	$1.71i \times 10^{1}$	-1.41×10^{-3}	$1.72i \times 10^{1}$	-1.72×10^{1}
		$[4^0, 4^0]$	2.92×10^{1}		2.39×10^{1}		2.94×10^{1}
		$[2^{+2}, 6^{-2}]$	-2.44×10^{-1}	$-2.25i \times 10^{-1}$	-9.49×10^{-3}	$-2.10i \times 10^{-1}$	1.91×10^{-1}
		$[2^0, 6^0]$	-5.73×10^{-1}		-4.29×10^{-1}		-4.77×10^{-1}
		$[0^0, 8^0]$	4.38×10^{-3}		3.00×10^{-3}		3.02×10^{-3}
	2	$[8^{+2}, 0^0]$	-2.61×10^{-1}		-1.72×10^{-1}		-1.70×10^{-1}
		$[6^{+4}, 2^{-2}]$	-1.97×10^{0}	$-1.97i \times 10^{0}$	1.57×10^{-1}	$-1.60i \times 10^{0}$	1.60×10^{0}
		$[6^{+2}, 2^0]$	-5.63×10^{0}		-4.16×10^{0}		-4.57×10^{0}
		$[6^0, 2^{+2}]$	-4.95×10^{0}	$4.96i \times 10^{0}$	3.95×10^{-1}	$4.01i \times 10^{0}$	4.01×10^{0}
		$[4^{+4}, 4^{-2}]$	-5.32×10^{0}	$-5.33i \times 10^{0}$	4.39×10^{-4}	$-5.35i \times 10^{0}$	5.36×10^{0}
		$[4^{+2}, 4^0]$	-2.09×10^{1}		-1.71×10^{1}		-2.11×10^{1}
		$[4^0, 4^{+2}]$	-2.38×10^{1}	$2.39i \times 10^{1}$	1.97×10^{-3}	$2.40i \times 10^{1}$	2.40×10^{1}
		$[4^{-2}, 4^{+4}]$	-8.57×10^{0}	$1.72i \times 10^{1}$	2.11×10^{1}	$-1.72i \times 10^{1}$	-8.64×10^{0}
		$[2^{+2}, 6^0]$	3.09×10^{-1}		2.31×10^{-1}		2.57×10^{-1}
		$[2^0, 6^{+2}]$	4.53×10^{-1}	$-4.18i \times 10^{-1}$	1.76×10^{-2}	$-3.91i \times 10^{-1}$	-3.55×10^{-1}
		$[2^{-2}, 6^{+4}]$	1.10×10^{-1}	$-1.97i \times 10^{-1}$	-2.11×10^{-1}	$1.48i \times 10^{-1}$	6.19×10^{-2}
		$[0, 8^{+2}]$	-3.44×10^{-3}	$2.93i \times 10^{-3}$	-2.38×10^{-4}	$2.55i \times 10^{-3}$	2.10×10^{-3}

The Cartesian product basis states in Eq. (6) are converted to the polar $|v_4^{l_4}, v_5^{l_5}\rangle$ basis by standard ladder operator methods.[54] Matrix elements are obtained from the relationship

$$\begin{aligned}\left|v_4^{l_4}, v_5^{l_5}\right\rangle &= \left[\left(\frac{v_4+l_4}{2}\right)!\left(\frac{v_4-l_4}{2}\right)!\left(\frac{v_5+l_5}{2}\right)!\left(\frac{v_5-l_5}{2}\right)!\right]^{-1/2} \\ &\times(\hat{a}_{4x}^\dagger + i\hat{a}_{4y}^\dagger)^{(v_4+l_4)/2}(\hat{a}_{4x}^\dagger - i\hat{a}_{4y}^\dagger)^{(v_4-l_4)/2} \\ &\times(\hat{a}_{5x}^\dagger + i\hat{a}_{5y}^\dagger)^{(v_5+l_5)/2}(\hat{a}_{5x}^\dagger - i\hat{a}_{5y}^\dagger)^{(v_5-l_5)/2}|0,0\rangle|0,0\rangle. \end{aligned} \tag{7}$$

The terms in the expansion of Eq. (7) are evaluated according to

$$\begin{aligned}&(\hat{a}_{4x}^\dagger)^{v_{4x}}(\hat{a}_{4y}^\dagger)^{v_{4y}}(\hat{a}_{5x}^\dagger)^{v_{5x}}(\hat{a}_{5y}^\dagger)^{v_{5y}}|0,0\rangle|0,0\rangle \\ &\quad = (v_{4x}!v_{4y}!v_{5x}!v_{5y}!)^{1/2}|v_{4x}, v_{4y}\rangle|v_{5x}, v_{5y}\rangle. \end{aligned} \tag{8}$$

The dominant contribution to the overlap integrals in the polar $|v_4^{l_4}, v_5^{l_5}\rangle$ basis will be proportional to the matrix elements for the basis transformation of Eq. (6). Let us ignore for a moment the constant prefactors and look only at the phases of the matrix elements, which arise from factors of $\pm i$ that multiply the in-plane ladder operators in Eq. (7). The general formula for the phase of the $\langle v_4^{l_4}, v_5^{l_5}|v_{4x}, v_{4y}\rangle|v_{4x}, v_{4y}\rangle$ matrix element is complicated. However, the expression is simple if we consider the matrix elements for the dominant overlap with the extreme members of the B^n polyad: $|0, v_{4y}\rangle|n, 0\rangle$ and $|0, v_{4y}\rangle|0, n\rangle$ for emission from 4^n and 6^n, respectively. For these cases, we obtain

$$\langle v_4^{l_4}, v_5^{l_5}|0, v_{4y}\rangle|n, 0\rangle \propto i^{(2v_4-l_4)} = i^{(2N_B-2v_5-l+l_5)}, \tag{9}$$

$$\langle v_4^{l_4}, v_5^{l_5}|0, v_{4y}\rangle|0, n\rangle \propto i^{(2v_4+2v_5-l_4-l_5)} = i^{(2N_B-l)}. \tag{10}$$

The matrix element in Eq. (9) for purely out-of-plane cis-bend excitation does not depend directly on v_5 or l_5 because the out-of-plane ladder operator $\hat{a}_{5x}^\dagger$ carries a phase of (+1). However, purely in-plane cis-bend excitation contributes a phase of $i^{2v_5-l_5}$ to Eq. (10), and as a result, the phase factor for the purely in-plane cis bend is a function of only N_B and l. That is, within a given pure bending polyad of the $\tilde{X}$ state, the predominant zero-order states that receive their brightness from the extreme 6^n member of the B^n polyad will all have the same phase. In the *gerade* pure bending polyads of the $\tilde{X}$ state, N_B and l are both even, so the phase factor will be +1 for $l = 0, 4, \ldots$ and −1 for $l = 2, 6, \ldots$ We expect overlap integrals from the extreme 4^n member of the B^n polyad to differ in phase by a factor of $i^{2v_5-l_5}$. We will return to this result in Sec. V B when we discuss the fluorescence intensities in the local mode basis.

The b_g members of the B^n polyads (with odd quanta of v_4' and v_6') have a different overlap pattern, which may be explained by symmetry considerations. Because b_g and a_g levels have vibrational wavefunctions with opposite total parity, the vibrational overlap integrals listed in Table V and in the supplementary material[53] from b_g levels are $\pi/2$ out-of-phase with those from a_g levels. However, because *a*- and *b*-axis Coriolis interactions between a_g and b_g vibrational levels must

preserve total parity, they couple rovibrational levels with opposite rotational parity, and the matrix elements for the Coriolis interactions are purely imaginary.[35] As we have noted, only the in-plane a_g component of v_4'' contributes to the FC overlap integral because the out-of-plane b_g component correlates with a rotation. Therefore, the vibrational symmetry of pure-bending S_0 levels in the overlap integral is determined by the contribution of v_5''. The *gerade* overtones of v_5'' have symmetry Σ_g^+ (for $l_5 = 0$), Δ_g (for $l_5 = 2$), Γ_g (for $l_5 = 4$), etc. In C_{2h}, Σ_g^+ correlates with A_g, whereas Δ_g and all higher-order *gerade* representations correlate with $A_g + B_g$. A consequence is that b_g members of the *gerade* B^n polyads may *only* fluoresce to states with $l_5 \neq 0$. For $l_4 + l_5 = 0$ levels of the $\tilde{X}$ state, B_g correlates with Σ_g^-, so fluorescence from a_g and b_g upper levels will reach $l = 0$ lower levels that differ in vibronic parity.

The different phases that are obtained for the vibrational overlap integrals in Table V lead to qualitatively different intensity patterns in the emission spectra from $\tilde{A}$-state B^n polyads to $\tilde{X}$-state bending polyads. This is because each zero-order bright state within the bending polyads of $\tilde{X}$ is fractionated into multiple different eigenstates by intrapolyad interactions.[22] Because the $v_5'' = v_4' + v_6'$ propensity rule will lead to brightness in more than one zero-order state of each pure bending polyad (of the type $|v_4^{l_4}, v_5^{l_5}\rangle = |(N_B - n)^{l_4}, n^{l_5}\rangle$ with different combinations of $l_4 + l_5 = l$), the intensity emitted into each eigenstate of the $\tilde{X}$-state pure bending polyads will result from constructive and destructive interferences between the contributions of various zero-order states that are bright in the spectrum, and the phases of the Franck-Condon overlap integrals will contribute in an important way. In our calculation, we have chosen the phases of the $\tilde{X}$-state normal modes to be consistent with the parameters of the $\tilde{X}$-state effective Hamiltonian reported by Herman and co-workers[21,23] and expanded by Jacobson and co-workers.[24,28,55]

The effective Hamiltonian parameters from Ref. 24 were used to calculate the fractionation of the zero-order states and simulate the emission spectra from zero-order members of the low-lying $\tilde{A}$-state B^n polyads (Figure 2). A few trends are visible in the simulated spectra. First, the overall intensity envelope increases dramatically with excitation in the $\tilde{X}$-state bending polyad, due to the favorable Franck-Condon contribution of v_4''. Overall intensity decreases with increasing quanta of B^n. Below $N_B = 12$, the eigenstates of the polyad are well described in the normal mode basis. In this regime, increasing the number of quanta of B^n in the upper level shifts the emission intensity envelope within each $\tilde{X}$-state bending polyad to higher frequency, because the nominal zero-order bright states obtained from the $v_5'' = v_4' + v_6'$ propensity rule contain more cis-bend character.

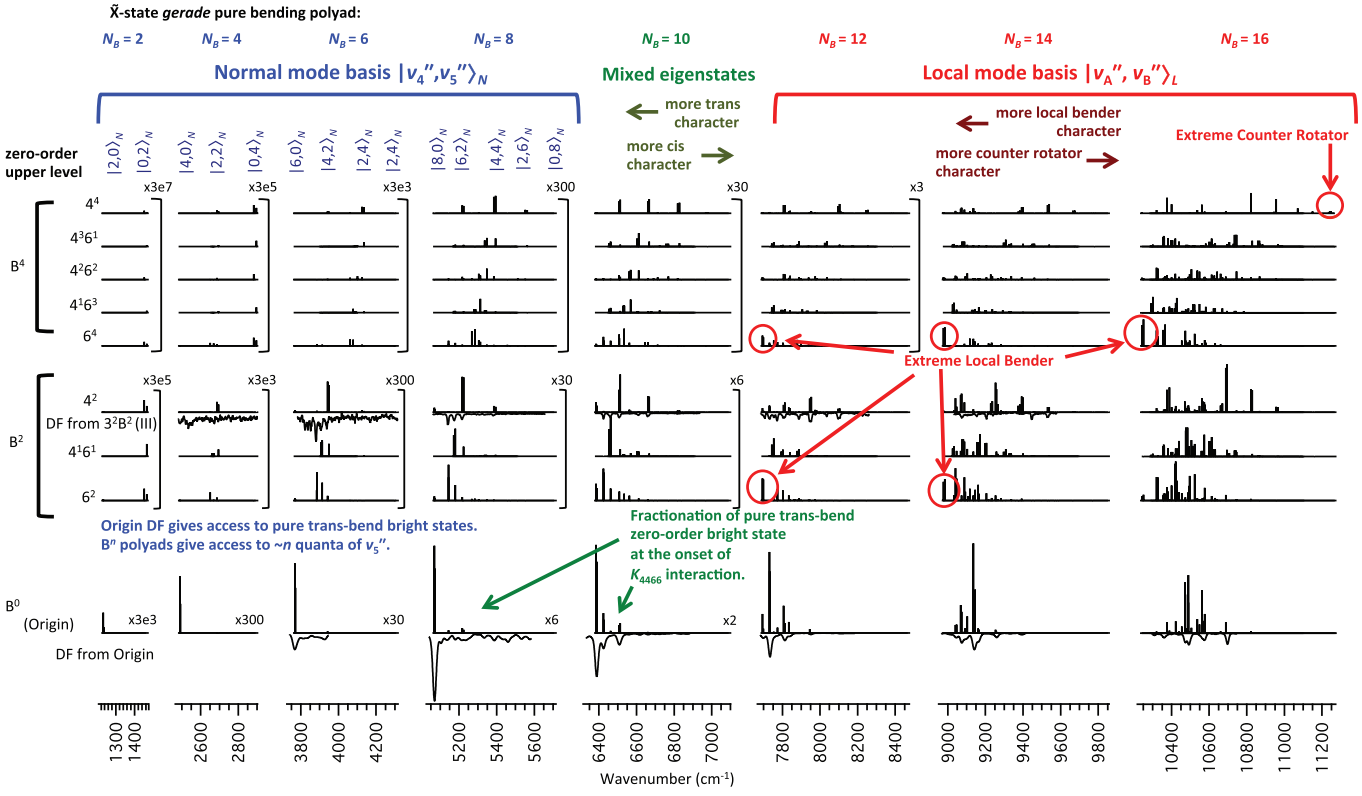

FIG. 2. Calculated emission intensities from zero-order members of low-lying B^n polyads of S_1 acetylene to pure bending polyads of S_0. The calculation takes into account interactions that occur within S_0 pure bending polyads, but ignores intra-polyad interactions in B^n. Vertical magnification (if any) is indicated to the right of each segment. The dispersed fluorescence spectrum from the highest-energy member of the 3^2B^2 polyad and the $\tilde{A}$-state origin are shown for comparison. Some features in the DF spectrum from 3^2B^2 (III) such as the peaks at 5140 and 5180 cm^{-1} may be explained through intrapolyad Darling-Dennison and *a*-axis Coriolis interactions within the 3^2B^2 polyad. At $N_B \geq 12$, the opposing anharmonicities of v_4'' and v_5'' cause strong Darling-Dennison interaction within the $\tilde{X}$-state bending polyads, leading to the emergence of new classes of motion. Eigenstates with extreme local bender character are intense in emission from upper levels with v_6' character and eigenstates with extreme counter-rotational character are intense in emission spectra from upper levels with v_4' character.

As N_B increases, there is an increase in the fractionation due to the Darling Dennison resonance K_{4466}, which leads to emergence of local mode eigenstates at $N_B \geq 12$. The different members of each B^n polyad start to give rise to qualitatively different interference patterns in the emission spectra. Above $N_B = 12$, $\tilde{A}$-state levels with the most v_6' character emit to the low-frequency end of the polyad where the eigenstates have the most large amplitude local bend character and levels with the most v_4' character emit to the high-frequency end of the polyad where the eigenstates have the most counter-rotational character. Emission from the $\tilde{A}$-state origin to the pure trans-bend bright state is fractionated among eigenstates in the center of the polyad, because in this regime the trans-bend is no longer a good basis function for describing of the motion encoded by the eigenstates.

B. Transformation of $\tilde{X}$-state intrapolyad pure bend intensities to the local mode basis

Access to the local bending zero-order states of $\tilde{X}$ may be calculated explicitly by performing a change of basis from the normal mode to the local mode basis. We will use the local mode definitions outlined by Jacobson and co-workers,[49] and the basis transformation described therein. Briefly, we label the CCH local bending modes A and B, and we define the local mode coordinates as linear combinations of the normal mode coordinates:

$$q_{Ax} = \frac{1}{\sqrt{2}}(q_{4x} + q_{5x}), \tag{11}$$

$$q_{Ay} = \frac{1}{\sqrt{2}}(q_{4y} + q_{5y}), \tag{12}$$

$$q_{Bx} = \frac{1}{\sqrt{2}}(-q_{4x} + q_{5x}), \tag{13}$$

$$q_{By} = \frac{1}{\sqrt{2}}(-q_{4y} + q_{5y}). \tag{14}$$

Because the bending amplitudes of v_4'' and v_5'' are well matched, this definition gives local bending modes that are almost (but not completely) localized in a single CCH bond angle. (The dimensionless normal coordinates used in this paper are scaled by the square root of the frequency, so the bending amplitudes will differ by a factor of $\sqrt{v_4''/v_5''}$, or approximately 8%.) From this definition, it is possible to derive local mode ladder operators

$$\hat{a}_{Ad} = \frac{1}{\sqrt{2}}(\hat{a}_{4d} + \hat{a}_{5d}), \tag{15}$$

$$\hat{a}_{Ag} = \frac{1}{\sqrt{2}}(\hat{a}_{4g} + \hat{a}_{5g}), \tag{16}$$

$$\hat{a}_{Bd} = \frac{1}{\sqrt{2}}(\hat{a}_{4d} - \hat{a}_{5d}), \tag{17}$$

$$\hat{a}_{Bg} = \frac{1}{\sqrt{2}}(\hat{a}_{4g} - \hat{a}_{5g}), \tag{18}$$

so that local mode basis states may be generated according to

$$(\hat{a}_{Ad}^{\dagger})^{n_{Ad}}(\hat{a}_{Ag}^{\dagger})^{n_{Ag}}(\hat{a}_{Bd}^{\dagger})^{n_{Bd}}(\hat{a}_{Bg}^{\dagger})^{n_{Bg}}|0^0, 0^0\rangle = \sqrt{n_{Ad}!n_{Ag}!n_{Bd}!n_{Bg}!}\,\left|n_A^{l_A}, n_B^{l_B}\right\rangle_L, \tag{19}$$

where

$$n_{Ad} = (n_A + l_A)/2, \tag{20}$$

$$n_{Ag} = (n_A - l_A)/2, \tag{21}$$

$$n_{Bd} = (n_B + l_B)/2, \tag{22}$$

$$n_{Bg} = (n_B - l_B)/2, \tag{23}$$

and the subscript L denotes that the state labels are in the local mode basis. A transformation from normal to local mode basis may be obtained by substituting Eqs. (15)–(18) into Eq. (19). However, the local mode basis states obtained in this manner will not be properly symmetrized with respect to either g/u inversion symmetry or total $+/-$ parity.

In the normal mode basis, the zero-order states have well-defined g/u symmetry, which is determined by the number of quanta of $v_5''(\pi_u)$. Normal mode basis states with well-defined $+/-$ symmetry are obtained by taking the linear combination

$$\left|n_4^{l_4}, n_5^{l_5}\right\rangle_N^{\pm} = \frac{1}{\sqrt{2}}\left(\left|n_4^{l_4}, n_5^{l_5}\right\rangle_N \pm \left|n_4^{-l_4}, n_5^{-l_5}\right\rangle_N\right). \tag{24}$$

We will use the N subscript to denote that the quantum numbers are in the normal mode basis. Local mode basis states may be symmetrized with respect to total $+/-$ parity in a similar manner,

$$\left|n_A^{l_A}, n_B^{l_B}\right\rangle_L^{\pm} = \frac{1}{\sqrt{2}}\left(\left|n_A^{l_A}, n_B^{l_B}\right\rangle_L \pm \left|n_A^{-l_A}, n_B^{-l_B}\right\rangle_L\right), \tag{25}$$

but states generated using Eq. (25) will still lack well-defined g/u symmetry. Symmetrization with respect to molecular-frame inversion may be obtained by interchanging the quantum numbers for the two local modes,

$$\left|n_A^{l_A}, n_B^{l_B}\right\rangle_L^{g/u} = \frac{1}{\sqrt{2}}\left(\left|n_A^{l_A}, n_B^{l_B}\right\rangle_L \pm \left|n_B^{l_B}, n_A^{l_A}\right\rangle_L\right), \tag{26}$$

where the $+$ combination corresponds to g symmetry and the $-$ combination corresponds to u symmetry. Both Eqs. (25) and (26) must be applied to achieve proper symmetrization, and the resulting symmetrized state will be a linear combination of up to four local mode basis states.

The normal to local mode basis transformation was applied to members of the pure bending polyads of the $\tilde{X}$ state in order to calculate the Franck-Condon access to local bending zero-order states. Within a polyad with $v_4'' + v_5'' = N_B$ and $l = 0$, the zero-order state undergoing the purest local bending motion will be $|N_B{}^0, 0^0\rangle_L$ (hereafter referred to as the "extreme local bender"), and the zero-order state undergoing the purest counter-rotational motion will be $|(N_B/2)^{N_B/2}, (N_B/2)^{-N_B/2}\rangle_L$ (hereafter referred to as the "extreme counter rotator").

Figures 3 and 4 show the emission intensity for transitions from the zero-order a_g members of $\tilde{A}$-state B^n polyads into the extreme local bender and the extreme counter rotator, respectively, of each pure bending polyad of the $\tilde{X}$ state, up to $N_B = 20$. Figure 3 also shows the total overall intensity into each pure bending polyad.

Some interesting trends are apparent in the figures. As n increases, the B^n polyads shift the overall FC envelope of

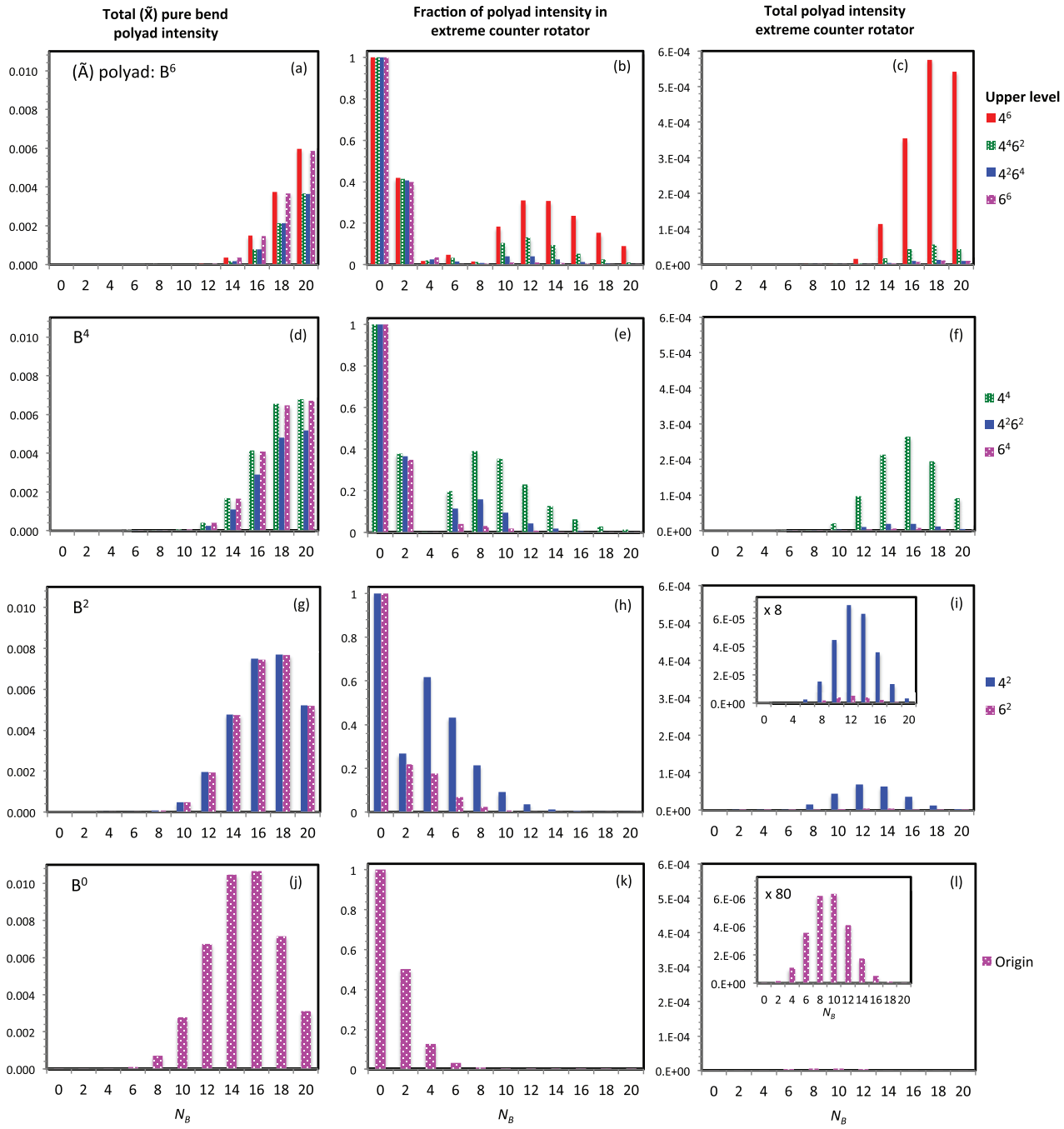

FIG. 3. (a)–(l) Calculated vibrational intensity for emission from a_g members of B^n polyads of Ã-state acetylene to pure bending polyads of the X̃ state with Σ_g^+ symmetry, illustrating access to the extreme counter rotator of each polyad. The first column gives the total overall intensity from each upper level to the X̃ state bending polyads. Column 2 gives the fraction of the total intensity in the extreme counter rotator zero-order state, $(|N_B/2^{N_B/2}, N_B/2^{-N_B/2}\rangle_L^{g+})$. Column 3 gives the total vibrational intensity in the extreme counter rotator zero-order state. For emission to a given X̃ state bending polyad, the quanta in ν_6' of the upper level increase from left to right, and the upper state levels are colored and textured according to the legend at the right.

the pure-bending polyads to higher energy (see column 1 of Figure 3), primarily because higher quanta in B^n provide Franck-Condon access to higher quanta of ν_5''. There appears to be a slight overall decrease in the amplitude of the FC envelope with increasing quanta of B^n, but for pure bending polyads of the X̃ state with the highest values of N_B, the total FC intensity *increases* with excitation in B^n.

Within an X̃-state pure bending polyad, the fraction of the bright state that corresponds to the extreme counter rotator (shown in the second column of Figure 3) depends only weakly on the identity of the Ã-state B^n polyad, but depends very sensitively on the number of quanta in ν_4'. As the number of quanta in ν_4' increases, access to the extreme counter rotator shifts to higher-lying polyads of the X̃ state, and the maximum counter rotational character is found in the polyad with approximately $N_B = 2\nu_4'$. On the other hand, the fraction of the bright state that corresponds to the extreme local bender (shown in the first column of Figure 4) depends very

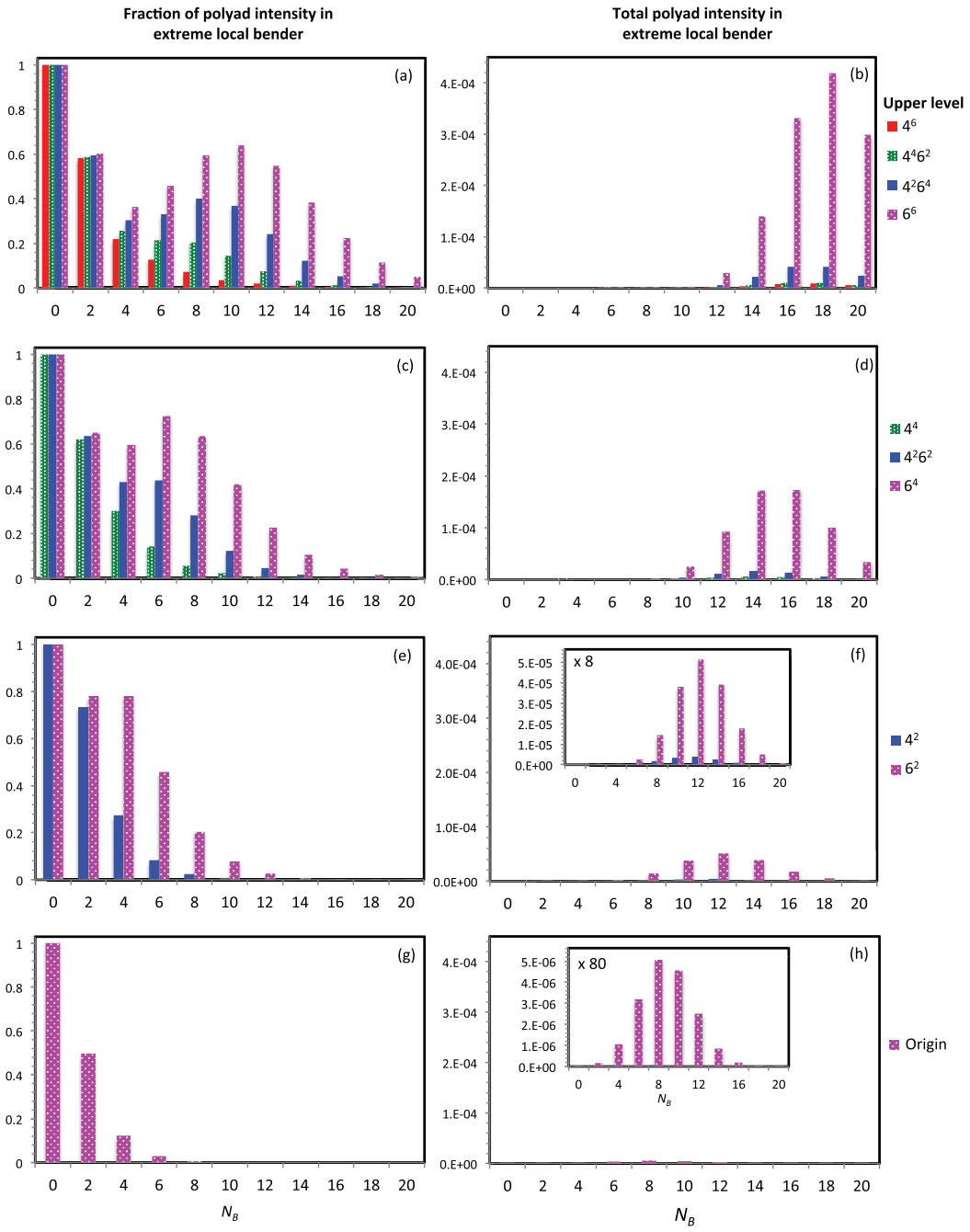

FIG. 4. (a)–(h) Calculated vibrational intensity for emission from a_g members of B^n polyads of Ã-state acetylene to the extreme local bender zero-order state, $(|N_B^0, 0^0\rangle_L^{g+})$, of each Σ_g^+ pure bending polyad of the X̃ state. The panels on the left side give the fraction of the total polyad intensity in the extreme local bender, and the panels on the right side give the total vibrational intensity in the extreme local bender. For emission to a given X̃ state bending polyad, the quanta in v_6' of the upper level increase from left to right, and the upper state levels are colored and textured according to the legend at the right.

sensitively on the number of quanta in v_6', and the maximum local bender character is found in the polyad with approximately $N_B = 2v_6'$.

This result is consistent with the FC propensity $v_5'' = v_4' + v_6'$ and with the fact that the pure local mode basis states require an equal combination of cis- and trans-bend character. When $N_B = 2n$, v_4'' and v_5'' will contribute equally to the character of the nominally-allowed zero-order bright states. The plurality of extreme counter rotational character obtained in bright states reached from v_4' overtones and extreme local bender character obtained in bright states reached from v_6' overtones increases with N_B. For example, although the extreme local bender character of the $N_B = 10$ polyad in the bright state accessed from 4^6 is only 64%, the rest of the intensity is fractionated among ten other zero-order states, and the state with the next-highest intensity $(|8^{+2}, 2^{-2}\rangle_L^{g+})$ carries only 14% of the brightness. This is why we see in Figure 2 that although emission from the Ã-state origin becomes increasingly fractionated at high N_B, the fractionation of the emission from the zero-order B^n levels may actually *decrease* slightly because the bright states that are accessed from these levels more closely resemble the character of the

eigenstates, which are better described in the local mode basis.

The extreme local bender is obtained from the vibrationless ground state via the ladder operator expression

$$\begin{aligned}\left|N_B^0, 0^0\right\rangle_L^{g+} &= \frac{1}{\sqrt{2}}\left[|N_B^0, 0^0\rangle_L + |0^0, N_B^0\rangle_L\right] \\ &= \frac{1}{\sqrt{2}}\left[(\hat{a}_{Ad}^\dagger)^{\frac{N_B}{2}}(\hat{a}_{Ag}^\dagger)^{\frac{N_B}{2}} + (\hat{a}_{Bd}^\dagger)^{\frac{N_B}{2}}(\hat{a}_{Bg}^\dagger)^{\frac{N_B}{2}}\right]|0^0 0^0\rangle \\ &= \frac{1}{2\sqrt{2}}\left[(\hat{a}_{4d}^\dagger + \hat{a}_{5d}^\dagger)^{\frac{N_B}{2}}(\hat{a}_{4g}^\dagger + \hat{a}_{5g}^\dagger)^{\frac{N_B}{2}}\right. \\ &\quad \left. + (\hat{a}_{4d}^\dagger - \hat{a}_{5d}^\dagger)^{\frac{N_B}{2}}(\hat{a}_{4g}^\dagger - \hat{a}_{5g}^\dagger)^{\frac{N_B}{2}}\right]|0^0 0^0\rangle. \end{aligned} \tag{27}$$

For integer $N_B/2$, the negative terms in Eq. (27) cancel so that all of the matrix elements for the transformation from the normal $|v_4^{l_4}, v_5^{l_5}\rangle_N$ basis to the extreme local bend, $|N_B^0, 0^0\rangle_L$, have the same constant phase factor of +1. On the other hand, the extreme counter rotator is obtained from

$$\begin{aligned}\left|\left(\frac{N_B}{2}\right)^{\frac{+N_B}{2}}, \left(\frac{N_B}{2}\right)^{\frac{-N_B}{2}}\right\rangle_L^{g+} &= \frac{1}{\sqrt{2}}\left[\left|\left(\frac{N_B}{2}\right)^{\frac{+N_B}{2}}, \left(\frac{N_B}{2}\right)^{\frac{-N_B}{2}}\right\rangle_L + \left|\left(\frac{N_B}{2}\right)^{\frac{-N_B}{2}}, \left(\frac{N_B}{2}\right)^{\frac{+N_B}{2}}\right\rangle_L\right] \\ &= \frac{1}{\sqrt{2}}\left[(\hat{a}_{Ad}^\dagger)^{\frac{N_B}{2}}(\hat{a}_{Bg}^\dagger)^{\frac{N_B}{2}} + (\hat{a}_{Ag}^\dagger)^{\frac{N_B}{2}}(\hat{a}_{Bd}^\dagger)^{\frac{N_B}{2}}\right]|0^0 0^0\rangle \\ &= \frac{1}{2}\left[(\hat{a}_{4d}^\dagger + \hat{a}_{5d}^\dagger)^{\frac{N_B}{2}}(\hat{a}_{4g}^\dagger - \hat{a}_{5g}^\dagger)^{\frac{N_B}{2}}\right. \\ &\quad \left. + (\hat{a}_{4g}^\dagger + \hat{a}_{5g}^\dagger)^{\frac{N_B}{2}}(\hat{a}_{4d}^\dagger - \hat{a}_{5d}^\dagger)^{\frac{N_B}{2}}\right]|0^0 0^0\rangle. \end{aligned} \tag{28}$$

Matrix elements from Eq. (28) carry a phase of $(-1)^{(v_5''+l_5)/2}$ for integer $N_B/2$. We have shown that the matrix element of the extreme local bender have the same relative phase as the bright state $|v_{4x}, v_{4y}\rangle|v_{5x}, v_{5y}\rangle = |0, v_{4y}\rangle|n, 0\rangle$ that is reached from 6^n (all phases are +1). The relative phases of the extreme counter rotator are not identical to the phases of the bright state $|0, v_{4y}\rangle|n, 0\rangle$ reached from 4^n, but there is a favorable amount of overlap, as evidenced in Figure 3.

In fact, from the relationship

$$\hat{a}_{4d}^\dagger = \frac{1}{\sqrt{2}}(\hat{a}_{4x}^\dagger + i\hat{a}_{4y}^\dagger), \tag{29}$$

$$\hat{a}_{5d}^\dagger = \frac{1}{\sqrt{2}}(\hat{a}_{5x}^\dagger + i\hat{a}_{5y}^\dagger), \tag{30}$$

$$\hat{a}_{4g}^\dagger = \frac{1}{\sqrt{2}}(\hat{a}_{4x}^\dagger - i\hat{a}_{4y}^\dagger), \tag{31}$$

$$\hat{a}_{5g}^\dagger = \frac{1}{\sqrt{2}}(\hat{a}_{5x}^\dagger - i\hat{a}_{5y}^\dagger), \tag{32}$$

we find the transformation from the Cartesian components of the normal mode basis to the extreme local bender,

$$\begin{aligned}\left|N_B^0, 0^0\right\rangle_L^{g+} &= \frac{1}{4}\{[(\hat{a}_{4x}^\dagger + \hat{a}_{5x}^\dagger)^2 + (\hat{a}_{4y}^\dagger + \hat{a}_{5y}^\dagger)^2]^{N_B/2} \\ &\quad + [(\hat{a}_{4x}^\dagger - \hat{a}_{5x}^\dagger)^2 + (\hat{a}_{4y}^\dagger - \hat{a}_{5y}^\dagger)^2]^{N_B/2}\}|0^0 0^0\rangle \end{aligned} \tag{33}$$

and the corresponding transformation to the extreme counter rotator,

$$\begin{aligned}&|(N_B/2)^{+N_B/2}, (N_B/2)^{-N_B/2}\rangle_L^{g+} \\ &= \frac{1}{4}\{[(\hat{a}_{4x}^\dagger + \hat{a}_{5x}^\dagger) + i(\hat{a}_{4y}^\dagger + \hat{a}_{5y}^\dagger)]^{N_B/2}[(\hat{a}_{4x}^\dagger - \hat{a}_{5x}^\dagger) - i(\hat{a}_{4y}^\dagger - \hat{a}_{5y}^\dagger)]^{N_B/2} \\ &\quad + [(\hat{a}_{4x}^\dagger + \hat{a}_{5x}^\dagger) - i(\hat{a}_{4y}^\dagger + \hat{a}_{5y}^\dagger)]^{N_B/2}[(\hat{a}_{4x}^\dagger - \hat{a}_{5x}^\dagger) + i(\hat{a}_{4y}^\dagger - \hat{a}_{5y}^\dagger)]^{N_B/2}\}|0^0 0^0\rangle. \end{aligned} \tag{34}$$

Inspection of Eq. (33) reveals that cross terms among the in-plane components will provide good overlap between the extreme local bender and the $|v_{4x}, v_{4y}\rangle|v_{5x}, v_{5y}\rangle = |0, v_{4y}\rangle|0, n\rangle$ bright state reached from 6^n, whereas inspection of Eq. (34) reveals that cross terms of $\hat{a}_{4y}$ with $\hat{a}_{5x}$ will provide good overlap between the extreme counter rotator and the $|0, v_{4y}\rangle|n, 0\rangle$ bright state reached from 4^n.

When viewed from a semi-classical perspective, this result is intuitive and unsurprising. When the trans-bent $\tilde{A}$-state acetylene molecule is displaced along the in-plane cis bend (q_6'), it reaches a half-linear geometry, which is exactly the classical turning point of the extreme local bending vibration in the $\tilde{X}$ state. By putting the correct number of quanta into ν_6', it should be possible to achieve good overlap with the extreme

local bend. We can expect the overlap to reach its maximum when the number of quanta in ν_6' are sufficient to reach the half-linear geometry at the classical turning point of the $\tilde{A}$-state vibration.

On the other hand, the extreme counter rotator has no amplitude at the linear geometry, but equal-and-opposite quanta of angular momentum in the two local bends. The classical analog of the motion along this mode involves circular motion of the two hydrogen atoms, in opposite directions. This is very similar to torsional motion in trans-bent $\tilde{A}$-state acetylene. At very high overtones of ν_4' (which have not been experimentally observed), we would expect the torsion to overcome the barrier to cis-trans isomerization, and the classical motion of the above barrier torsion will be very similar to that of the $\tilde{X}$-state extreme counter rotator.

It may be possible to enhance the brightness of FC intensity into large amplitude extreme local benders by adding quanta of the trans bend, ν_3'. Quanta of trans-bend dramatically increase the overall intensity of the $\tilde{A}$—$\tilde{X}$ transition because of the large-amplitude displacement between the two equilibria along the trans-bending coordinate. Furthermore, $\nu_3' + \nu_6'$ samples the cis↔trans isomerization on the S_1 surface, and the half-linear transition state geometries for the S_1 cis↔trans isomerization and the S_0 acetylene↔vinylidene isomerization are believed to be similar.[42,56] Thus if we follow the isomerization coordinate on the S_1 surface, it will give access to large amplitude local bending levels that sample the transition state geometry for the isomerization on the S_0 surface. Moreover, the cis↔trans isomerization causes ν_3' to have a large x_{36} cross-anharmonicity with ν_6' that decouples ν_6' from the B^n polyads.[36,42–44,50] As a result, ν_3' not only enhances FC intensity to large amplitude local bend ZOBSs, but it should also give rise to 3^m6^n perfect pluck levels that are relatively unsullied by intrapolyad interactions with levels of ν_4' character, which have been ignored in the present calculation. A forthcoming paper will discuss the effects of $\tilde{A}$-state anharmonic interactions on the emission intensities.

VI. CONCLUSIONS

Our FC calculation for the $\tilde{A}$—$\tilde{X}$ system of acetylene is done in the harmonic basis, so we do not expect quantitative agreement, especially at high vibrational energies where anharmonic effects become important. However, we have shown that a simple computational method can reproduce qualitative trends in the spectrum and correctly explain observed interference effects. The calculation provides physical explanations for initially puzzling observations, while also uncovering new insights into Franck-Condon propensity rules that will hopefully guide ongoing areas of research. Our results suggest that the search for "local-bender pluck" eigenstates of S_1 acetylene that will grant the best access to local benders in S_0 should focus on states with many quanta in ν_6'. Adding quanta of ν_3' is also likely to improve the FC intensity.

The application of a-axis Eckart constraints to the full-dimensional vibrational overlap integral in the $\tilde{A}$—$\tilde{X}$ system of acetylene removes the out-of-plane component of the trans bend from the vibrational overlap integral. This affects the structure of the coordinate transformation and the symmetry properties of the wavefunctions that participate in the integral, but the consequences have been neglected by previous investigators. Furthermore, because of the generality of the method developed in Paper I[57] for polyatomic linear-bent transitions—provided that the FC integral does not accumulate near the linear geometry—we predict that analogous consequences should appear in the Franck-Condon propensities of other linear-bent systems. In general, application of the a-axis Eckart constraint for the linear molecule (restoring the χ Euler angle) will remove one of the degrees of freedom from the bending vibrations of the linear molecule, and this degree of freedom will not contribute to the Franck-Condon integral away from linear geometry. The effect of the Eckart constraint on the vibrational degrees of freedom will depend on the structure of the molecule in the linear and nonlinear states, but it will always lead to FC propensity rules involving the bending modes of the linear molecule.

Our calculations suggest that the FC intensity for emission into the ν_5'' cis bend is also best viewed in the Cartesian in-plane vs. out-of-plane basis rather than the polar basis (with v, l quantum numbers), because the properties of the trans-bent $\tilde{A}$-state give rise to a simple propensity rule for each Cartesian component of ν_5'' (Eq. (6)). The propensity rules in Eq. (6) are more specific than the $v_5'' = v_4' + v_6'$ propensity rule, and may be used to predict the exact zero-order bright state composition in any basis. To our knowledge, the FC propensities into the Cartesian components of ν_5'' have not been discussed by previous authors.

ACKNOWLEDGMENTS

G.B.P. would like to thank P. Bryan Changala, and Jun Jiang for valuable discussions. We would like to thank Professor Kaoru Yamanouchi and Dr. Richard Duan for sharing their raw dispersed fluorescence data. This material is based upon work supported by the U.S. Department of Energy, Office of Science, Chemical Sciences Geosciences and Biosciences Division of the Basic Energy Sciences Office, under Award No. DE-FG0287ER13671.

[1]G. W. King and C. K. Ingold, Nature (London) **169**(4313), 1101–1102 (1952).
[2]C. K. Ingold and G. W. King, J. Chem. Soc. **1953**, 2702–2755 (1953).
[3]K. K. Innes, J. Chem. Phys. **22**(5), 863–876 (1954).
[4]E. K. Plyler, E. D. Tidwell, T. A. Wiggins, J. Opt. Soc. Am. **53**, 589–593 (1963).
[5]J. Plíva, J. Mol. Spectrosc. **44**(1), 145–164 (1972).
[6]K. F. Palmer, M. E. Mickelson, and K. N. Rao, J. Mol. Spectrosc. **44**(1), 131–144 (1972).
[7]A. Baldacci, S. Ghersetti, and K. N. Rao, J. Mol. Spectrosc. **68**(2), 183–194 (1977).
[8]A. Baldacci, S. Ghersetti, and K. N. Rao, J. Mol. Spectrosc. **41**(1), 222–225 (1972).
[9]L. Sinitsa, J. Mol. Spectrosc. **84**(1), 57–59 (1980).
[10]B. C. Smith and J. S. Winn, J. Chem. Phys. **89**(8), 4638–4645 (1988).
[11]J. K. G. Watson, M. Herman, J. C. V. Craen, and R. Colin, J. Mol. Spectrosc. **95**(1), 101–132 (1982).
[12]J. C. V. Craen, M. Herman, R. Colin, and J. K. G. Watson, J. Mol. Spectrosc. **111**(1), 185–197 (1985).
[13]J. C. V. Craen, M. Herman, R. Colin, and J. K. G. Watson, J. Mol. Spectrosc. **119**(1), 137–143 (1986).
[14]M. Herman, T. Huet, and M. Vervloet, Mol. Phys. **66**(2), 333–353 (1989).

[15]W. Lafferty and A. Pine, J. Mol. Spectrosc. **141**(2), 223–230 (1990).
[16]R. D'Cunha, Y. Sarma, G. Guelachvili, R. Farrenq, Q. Kou, V. Devi, D. Benner, and K. N. Rao, J. Mol. Spectrosc. **148**(1), 213–225 (1991).
[17]A.-M. Tolonen and S. Alanko, Mol. Phys. **75**(5), 1155–1165 (1992).
[18]Y. Kabbadj, M. Herman, G. D. Lonardo, L. Fusina, and J. Johns, J. Mol. Spectrosc. **150**(2), 535–565 (1991).
[19]J. Vanderauwera, D. Hurtmans, M. Carleer, and M. Herman, J. Mol. Spectrosc. **157**(2), 337–357 (1993).
[20]Q. Kou, G. Guelachvili, M. A. Temsamani, and M. Herman, Can. J. Phys. **72**(11–12), 1241–1250 (1994).
[21]M. A. Temsamani and M. Herman, J. Chem. Phys. **102**(16), 6371–6384 (1995).
[22]S. A. B. Solina, J. P. O'Brien, R. W. Field, and W. F. Polik, J. Phys. Chem. **100**(19), 7797–7809 (1996).
[23]M. A. Temsamani, M. Herman, S. A. B. Solina, J. P. O'Brien, and R. W. Field, J. Chem. Phys. **105**(24), 11357–11359 (1996).
[24]M. P. Jacobson, J. P. O'Brien, R. J. Silbey, and R. W. Field, J. Chem. Phys. **109**(1), 121–133 (1998).
[25]M. P. Jacobson, C. Jung, H. S. Taylor, and R. W. Field, J. Chem. Phys. **111**(2), 600–618 (1999).
[26]M. I. El Idrissi, J. Liévin, A. Campargue, and M. Herman, J. Chem. Phys. **110**(4), 2074–2086 (1999).
[27]M. P. Jacobson and R. W. Field, J. Phys. Chem. A **104**(14), 3073–3086 (2000).
[28]K. Hoshina, A. Iwasaki, K. Yamanouchi, M. P. Jacobson, and R. W. Field, J. Chem. Phys. **114**(17), 7424–7442 (2001).
[29]M. Herman, A. Campargue, M. I. E. Idrissi, and J. V. Auwera, J. Phys. Chem. Ref. Data **32**(3), 921–1361 (2003).
[30]J. D. Tobiason, A. L. Utz, and F. F. Crim, J. Chem. Phys. **99**(2), 928–936 (1993).
[31]A. L. Utz, J. D. Tobiason, E. Carrasquillo, L. J. Sanders, and F. F. Crim, J. Chem. Phys. **98**(4), 2742–2753 (1993).
[32]M. Mizoguchi, N. Yamakita, S. Tsuchiya, A. Iwasaki, K. Hoshina, and K. Yamanouchi, J. Phys. Chem. A **104**(45), 10212–10219 (2000).
[33]A. J. Merer, N. Yamakita, S. Tsuchiya, J. F. Stanton, Z. Duan, and R. W. Field, Mol. Phys. **101**(4–5), 663–673 (2003).
[34]A. H. Steeves, A. J. Merer, H. A. Bechtel, A. R. Beck, and R. W. Field, Mol. Phys. **106**(15), 1867–1877 (2008).
[35]A. J. Merer, N. Yamakita, S. Tsuchiya, A. H. Steeves, H. A. Bechtel, and R. W. Field, J. Chem. Phys. **129**(5), 054304 (2008).
[36]A. H. Steeves, H. A. Bechtel, A. J. Merer, N. Yamakita, S. Tsuchiya, and R. W. Field, J. Mol. Spectrosc. **256**(2), 256–278 (2009).
[37]A. J. Merer, A. H. Steeves, J. H. Baraban, H. A. Bechtel, and R. W. Field, J. Chem. Phys. **134**(24), 244310 (2011).
[38]K. M. Ervin, J. Ho, and W. C. Lineberger, J. Chem. Phys. **91**(10), 5974–5992 (1989).
[39]S. Joseph and A. J. C. Varandas, J. Phys. Chem. A **114**(50), 13277–13287 (2010).
[40]S. Zou and J. M. Bowman, Chem. Phys. Lett. **368**(3–4), 421–424 (2003).
[41]H. Lee, J. H. Baraban, R. W. Field, and J. F. Stanton, J. Phys. Chem. A **117**(46), 11679–11683 (2013).
[42]J. H. Baraban, A. R. Beck, A. H. Steeves, J. F. Stanton, and R. W. Field, J. Chem. Phys. **134**(24), 244311 (2011).
[43]P. B. Changala, J. H. Baraban, J. F. Stanton, A. J. Merer, and R. W. Field, J. Chem. Phys. **140**(2), 024313 (2014).
[44]J. H. Baraban, A. J. Merer, J. F. Stanton, and R. W. Field, Mol. Phys. **110**(21–22), 2725–2733 (2012).
[45]K. Tsuji, C. Terauchi, K. Shibuya, and S. Tsuchiya, Chem. Phys. Lett. **306**(1–2), 41–47 (1999).
[46]J. K. G. Watson, J. Mol. Spectrosc. **207**(2), 276–284 (2001).
[47]J. Jiang, J. H. Baraban, G. B. Park, M. L. Clark, and R. W. Field, J. Phys. Chem. A **117**(50), 13696–13703 (2013).
[48]J. D. Tobiason, A. L. Utz, E. L. Sibert, and F. F. Crim, J. Chem. Phys. **99**(8), 5762–5767 (1993).
[49]M. P. Jacobson, R. J. Silbey, and R. W. Field, J. Chem. Phys. **110**(2), 845–859 (1999).
[50]J. H. Baraban, P. B. Changala, A. J. Merer, A. H. Steeves, H. A. Bechtel, and R. W. Field, Mol. Phys. **110**(21–22), 2707–2723 (2012).
[51]V. Tyng and M. E. Kellman, J. Phys. Chem. B **110**(38), 18859–18871 (2006).
[52]See http://pages.uoregon.edu/meklab/migration2/ for animations illustrating the classical motions that result from the normal-to-local mode bifurcation on the ground electronic surface of acetylene.
[53]See supplementary material at http://dx.doi.org/10.1063/1.4896533 for a table of signed overlap integrals relevant to the pure-bending emission spectrum.
[54]C. Cohen-Tannoudji, B. Diu, and F. Laloë, *Quantum Mechanics* (Hermann, Paris, France, 1977).
[55]M. P. Jacobson, J. P. O'Brien, and R. W. Field, J. Chem. Phys. **109**(10), 3831–3840 (1998).
[56]B. M. Wong, A. H. Steeves, and R. W. Field, J. Phys. Chem. B **110**(38), 18912–18920 (2006).
[57]G. B. Park, J. H. Baraban, and R. W. Field, J. Chem. Phys. **141**, 134304 (2014).